Precise Flight-Path Control Using a Predictive Algorithm

Y. C. Jung* and R. A. Hess†
University of California, Davis, Davis, California 95616

Generalized predictive control describes an algorithm for the control of dynamic systems in which a control input is generated that minimizes a quadratic cost function consisting of a weighted sum of errors between desired and predicted future system output and future predicted control increments. The output predictions are obtained from an internal model of the plant dynamics. A design technique is discussed for applying the single-input/single-output generalized predictive control algorithm to a problem of longitudinal/vertical terrain-following flight of a rotorcraft. By using the generalized predictive control technique to provide inputs to a classically designed stability and control augmentation system, it is demonstrated that a robust flight-path control system can be created that exhibits excellent tracking performance.

Introduction

OVER the past decade, a general technique has been introduced for the design of automatic controllers, called variously, model predictive heuristic control, model algorithmic control, output predictive control, dynamic matrix control, etc.[1-4] More recently, Clarke and Zhang[4] and Clarke et al.[5] have introduced generalized predictive control (GPC) and have related it to the earlier approaches of Refs. 1–4 and linear quadratic (LQ) designs and have incorporated self-tuning into the control algorithm. Cast in terms of the flight-path control problem that will be the subject of the research to be described, the GPC algorithm, formulated as a discrete control problem, can be summarized as follows.[6]

1) At each present time instant t_k, a prediction of the vehicle path j sampling periods into the future is made. This prediction is obtained from a model of the vehicle dynamics.

2) A control strategy for the next N_U sampling intervals is selected, which brings the predicted vehicle path back to a desired path in the best way according to a specific control objective, i.e., LQ, or model following, etc.

3) The resulting best control is then applied but only over the next sampling interval, and at the next sampling instant the procedure is repeated, which results in a continuously updated control action with corrections based on the latest measurements.

Hess and Jung[7] have shown the potential performance of a GPC design in a rotorcraft longitudinal vertical flight-path control problem using simplified vehicle dynamics. The research to be described herein demonstrates how the single-input/single-output (SISO) GPC algorithm might be incorporated into a flight-path control system to obtain a robust design with excellent performance.

Generalized Predictive Control Algorithm

Details of the GPC algorithm, itself, can be found in Ref. 5; however, a brief review of the salient features of the approach will be undertaken in what follows.

The plant is modeled in discrete fashion using the so-called Controlled Auto-Regressive Integrated Moving Average model[5]:

$$A(q^{-1})y(t) + B(q^{-1})u(t-1) + \xi(t)/\Delta \tag{1a}$$

$$A(q^{-1}) = 1 + a_1 q^{-1} + \cdots + a_{na} q^{-na} \tag{1b}$$

$$B(q^{-1}) = b_0 + b_1 q^{-1} + \cdots + b_{nb} q^{-nb} \tag{1c}$$

where q^{-1} is the delay operator, $y(t)$ and $u(t)$ the output and control variables, respectively; $\xi(t)$ is an uncorrelated random sequence; and Δ the differencing operator $(1 - q^{-1})$. The actual sampling interval is T, so that, at each sampling instant, the independent variable in Eqs. (1) is kT. Now, a prediction of the plant output, given measured output up to time kT and known control input $u(t+i)$ for $i \leq -1$, is

$$\hat{y}(t+j\,|\,t) = E_j(q^{-1})B(q^{-1})\Delta u(t+j-1) + F_j(q^{-1})y(t) \tag{2}$$

where j is the number of future time steps being predicted, and $E_j(q^{-1})$ and $F_j(q^{-1})$ the result from a recursive solution of the Diophantine identity[8]

$$1 = E_j(q^{-1})A(q^{-1})\Delta + q^{-j}F_j(q^{-1}) \tag{3}$$

Also,

$$E_j(q^{-1})B(q^{-1}) = G_j(q^{-1}) + q^{-j}\Gamma_j(q^{-1}) \tag{4}$$

where

$$G_j(q^{-1}) = g_0 + g_1 q^{-1} + \cdots + g_{j-1} q^{-j+1} \tag{5a}$$

$$\Gamma_j(q^{-1}) = \gamma_{j,0} + \gamma_{j,1} q^{-1} + \cdots + \gamma_{j,nb-1} q^{-nb+1} \tag{5b}$$

Substitution of Eq. (4) into Eq. (2) results in

$$\begin{aligned}\hat{y}(t+j\,|\,t) &= G_j(q^{-1})\Delta u(t+j-1) + \Gamma_j(q^{-1})\Delta u(t-1) + F_j(q^{-1})y(t) \\ &= G_j(q^{-1})\Delta u(t+j-1) + y^{oL}(t+j)\end{aligned} \tag{6}$$

with

$$y^{oL}(t+j) = \Gamma_j(q^{-1})\Delta u(t-1) + F_j(q^{-1})y(t) \tag{7}$$

Now a predictive control law can be defined as that which minimizes a cost function given by

$$J(N_1,N_2) = E\left\{\sum_{j=N_1}^{N_2}[y(t+j) - w(t+j)]^2 + \sum_{j=1}^{N_2}\lambda(j)[\Delta u(t+j-1)^2]\right\} \tag{8}$$

Received Feb. 23, 1989; revision received June 26, 1990; accepted for publication June 26, 1990.

*Graduate Student, Department of Mechanical, Aeronautical, and Materials Engineering.

†Professor, Department of Mechanical, Aeronautical, and Materials Engineering. Associate Fellow AIAA.

where N_1 is the minimum costing horizon, N_2 the maximum costing horizon, $w(k)$ the desired value of the output y at the kth sampling instant, and $\lambda(j)$ a control weighting sequence.

Equation (8) is concerned only with a subset of future time defined N_2T s into the future and is dependent upon data up to time kT. As outlined earlier, the control is generated in the following manner: at each sampling instant, an optimal control sequence for N_2 steps into the future is calculated; however, only the first of these is applied to the plant. At the next sampling instant, a new optimal sequence is calculated that minimizes J for N_2 steps into the future, but again, only the first of these is applied to the plant. This defines a "receding horizon" strategy.

Significant reductions in the order of the matrices involved in computing the optimal control can be made by requiring that, after an interval $N_U < N_2$, projected control increments are assumed to be zero, i.e.,

$$\Delta u(t+j-1) = 0, \qquad j > N_U \tag{9}$$

where N_U is called the "control horizon." This procedure is equivalent to placing infinite weights on control increments after a future time $N_U \cdot T$. With the introduction of the control horizon, the prediction equations become

$$\hat{y} = G_1\tilde{u} + y^{oL} \tag{10}$$

where

$$G_1 = \begin{bmatrix} g_0 & 0 & 0 & \cdots & 0 \\ g_1 & g_0 & 0 & & 0 \\ \cdot & \cdot & \cdot & \cdots & \cdot \\ \cdot & \cdot & \cdot & \cdots & \cdot \\ g_{N-1} & g_{N-2} & g_{N-3} & & g_{N-N_U} \end{bmatrix}_{(N \times N_U)} \tag{11a}$$

$$\hat{y} = [\hat{y}(t+1), \hat{y}(t+2), \ldots, \hat{y}(t+N)]^T \tag{11b}$$

$$\tilde{u} = [\Delta u(t), \Delta u(t+1), \ldots, \Delta u(t+N_U-1)]^T \tag{11c}$$

$$y^{oL} = [y^{oL}(t+1), y^{oL}(t+2), \ldots, y^{oL}(t+N)]^T \tag{11d}$$

For simplicity of notation, it was assumed in Eqs. (11) that $N_1 = 1$ and N_2 was referred to simply as N. The corresponding control law is given by

$$\tilde{u} = (G_1^T G_1 + \lambda I)^{-1} G_1^T (w - y^{oL}) \tag{12}$$

$$\Delta u(t) = k^T (w - y^{oL}) \tag{13a}$$

$$k^T = [1,0,0,\ldots,0](G_1^T G_1 + \lambda I)^{-1} G_1^T \tag{13b}$$

The current control law $u(k)$ is thus

$$u(t) = u(t-1) + k^T (w - y^{oL}) \tag{14}$$

The incremental controller ensures zero offset even with nonzero disturbances and, as such, is equivalent to integral control.

The final products of the entire GPC design are contained in the coefficients of the $\Gamma_j(q^{-1})$ and $G_j(q^{-1})$ polynomials of Eqs. (5) and in the elements of the k matrix of Eq. (14), all of which can be precomputed.

The choice of parameters N_1, N_2, N_U, T, and λ determines the performance and stability of the GPC algorithm. It will be demonstrated how guidelines for selecting these parameters[9] can be incorporated into an overall design procedure. Regarding stability, the following theorem is of interest[9]:

Given: A state-space model of the plant of Eqs. (1), augmented by an integrator:

$$x(t+1) = Ax(t) + b\Delta u(t) \tag{15a}$$

$$y(t) = c^T x(t) \tag{15b}$$

The state-space model of Eqs. (15) is stable under GPC control if

1) The n-state model (A,b,c) is stabilizable and detectable, and if

2) $NU = N_1 \geq n$, $N_2 - N_1 \geq n - 1$, and $\lambda = \epsilon \to 0$.

A proof of this theorem is offered in Ref. 9. As will be seen, conditions 1 and 2 will, in general, be met by the proposed application of the GPC algorithm.

Analysis of Single-Input/Single-Output Generalized Predictive Control Designs

Substituting Eq. (7) into Eqs. (13a) gives

$$\Delta u(t) = \sum_{i=N_1}^{N_2} k_i q^i w(t) - \sum_{i=N_1}^{N_2} k_i \Gamma_i(q^{-1})\Delta u(t-1) - \sum_{i=N_1}^{N_2} k_i F_i(q^{-1}) y(t) \tag{16}$$

or

$$\left[1 + q^{-1}\sum_{N_1}^{N_2} k_i \Gamma_i(q^{-1})\right]\Delta u(t) = \sum_{N_1}^{N_2} k_i q^i w(t) - \sum_{N_1}^{N_2} k_i F_i(q^{-1}) y(t) \tag{17}$$

Equation (17) can be represented in the form of the block diagram shown in Fig. 1.[10] The closed-loop transfer function can be obtained directly as

$$\frac{y}{w}(q^{-1}) = \frac{[\sum k_i q^i q^{-1} B(q^{-1})]/(1-q^{-1})[1+q^{-1}\sum k_i \Gamma_i] A(q^{-1})}{1 + \{[q^{-1}B(q^{-1})\sum k_i F_i(q^{-1})]/(1-q^{-1})[1+q^{-1}\sum k_i \Gamma_i] A(q^{-1})\}} \tag{18}$$

with the loop transmission given by

$$L(q^{-1}) = \frac{q^{-1}B(q^{-1})\sum k_i F_i(q^{-1})}{(1-q^{-1})[1+q^{-1}\sum k_i \Gamma_i] A(q^{-1})} \tag{19}$$

By transforming into the w' plane, the Bode plot of Eq. (19) allows the phase and gain margins of the SISO GPC controlled system to be examined just as with a conventional, nonpredictive SISO design.

Design Procedure

Figure 2 shows how the SISO GPC algorithm could be incorporated into a multi-input/multi-output (MIMO) flight control system. Here, is it assumed that mission/task requirements demand very precise tracking performance for one of the output variables (shown here as y). An example would be vertical flight-path deviations in a terrain-following flight task. It is this hypothesized stringent performance requirement that justifies the use of the GPC algorithm as part of the flight control system.

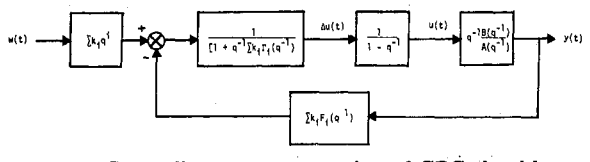

Fig. 1 Block diagram representation of GPC algorithm.

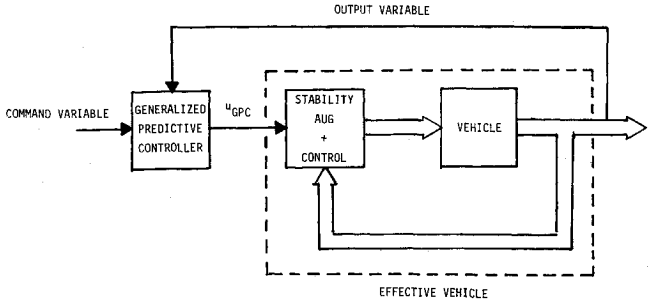

Fig. 2 Incorporating the SISO GPC algorithm into a MIMO flight control system.

The proposed design procedure would require, in most applications, that the vehicle possess a stability augmentation system (SAS). We would include in the definition of SAS here, control of other pertinent output variables not subject to GPC control. From the standpoint of the GPC design, the purpose of this SAS is to 1) provide stabilizable and detectable dynamics, i.e., to ensure that modes that may not be controllable or observable are at least asymptotically stable; 2) reduce the variations in the dynamics of the "effective vehicle" over the flight regime in which the GPC design is to be used; 3) reduce the effects of any nonlinearities in the vehicle dynamics; and 4) simplify the vehicle dynamics, i.e., reduce the apparent order of the transfer function for the effective vehicle that is used in determining the GPC control law. Thus, in the overall design, the SAS will provide robustness; the GPC, performance. Since most high-performance flight vehicles now include a full-authority SAS for acceptable handling qualities, this approach appears quite reasonable. As will be seen, a properly designed SAS can allow a single, fixed-parameter GPC design to control a vehicle over a flight regime in which the unaugmented dynamics are subject to considerable variation.

The design procedure can be summarized as follows.

1) Create an "effective vehicle" that possesses the desirable dynamic characteristics outlined earlier. This effective vehicle typically will be obtained using linear feedback principles associated with any acceptable feedback design technique, e.g., H^∞ (Ref. 11) or the quantitative feedback theory (QFT).[12] Note that system performance is not the object of this design.

2) Referring to Fig. 2, form the $y(s)/u_{GPC}(s)$ transfer function, with the feedback loops obtained in step 1 closed.

3) If possible, approximate the $y(s)/u_{GPC}(s)$ of step 2, with a lower order transfer function. Discretize this transfer function, including a zero-order hold. Here the discretization interval T is assumed to be dictated by constraints other than the control system design, e.g., minimum cycle time of the digital computer implementing the GPC law.

4) Select the initial GPC parameters as follows[9]: $N_1 = n$, the order of the discretized transfer function from step 3, plus one, to account for the integral action of the GPC design; $N_2 = 2n - 1$; $N_U = n$; $\lambda = \epsilon$, a value large enough to ensure invertibility in the matrix $\boldsymbol{G}_1^T\boldsymbol{G}_1 + \lambda\boldsymbol{I}$ in Eq. (12). Thus, here the weighting sequence of Eq. (8) is a constant value.

5) With these selections, and using unit step responses, adjust λ by trial and error, to ensure stability, desirable transient performance, and adequate gain and phase margins. Of course, this trial and error is equivalent to a pole-placement procedure and the problem can be approached as such. For this step, use the simplified transfer function of step 3.

6) Evaluate the GPC law obtained in step 5, again using unit step responses, however, now using the complete vehicle/SAS model. If the GPC design to this point is acceptable, simulate by using more realistic command inputs over the entire flight regime of interest. If the design is not acceptable, repeat steps 3-6, with a more accurate simplified transfer function. It may be necessary to modify the values of N_2 and N_U, so that $N_2 > 2n - 1$ and $N_U > n$.[9] Finally, of course, the flight regime may involve changes in vehicle characteristics of such magnitude that GPC control law scheduling may be necessary.

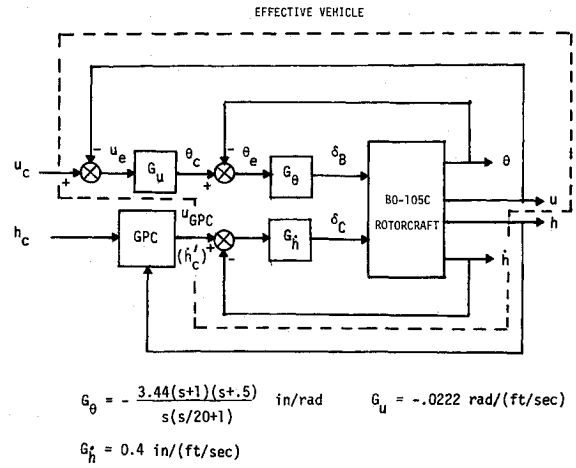

Fig. 3 Stability augmentation system for BO-105C vehicle.

Design Example

Task and Vehicle Model

The example to be presented involves a rotorcraft terrain-following task. This task is also often referred to as "contour flight" and is characterized by low-altitude flight conforming generally to the contours of the terrain and gross vegetation features. Each leg of contour flight is characterized by constant heading, varying airspeed, and flight path as close to the Earth's surface as vegetation, obstacles, and ambient light will permit.[13] The rotorcraft model for this study is a rigid-body model of the BO-105C.[14] To provide a challenging task, the command airspeed ranged from 20 to 100 kts while the vehicle was to follow a vertical flight path emulating a precomputed profile described by a sum of three sinusoids:

$$h_c(t) = w(t) = 20\{\sin[0.05(2\pi t)] + \sin[0.06(2\pi t)] + \sin[0.08(2\pi t)]\} \quad \text{ft} \tag{20}$$

The Appendix describes the vehicle model. Basically, the dynamics were obtained through linear interpolation between five equilibrium flight conditions at 20, 40, 60, 80, and 100 kts. The interpolation was based on low-pass filtered vehicle airspeed. The command airspeed profile consisted of a series of constant accelerations of 3.375 ft/s^2 for 10 s each, followed by 10 s of constant velocity. The constant-velocity sections occurred at 20, 40, 60, 80, and 100 kts, respectively. The unaugmented vehicle dynamics were linear, but time-varying, highly coupled, and, depending on the airspeed, unstable and/or nonminimum phase in nature. The coupling referred to here is that between attitude and vertical velocity.

Design

1) Figure 3 shows the SAS designed to meet the aforementioned criteria. We include airspeed control as part of this SAS design. The design was a "classical" frequency-domain approach involving successive loop closures, beginning with pitch attitude, then altitude rate, and finally airspeed. The airspeed loop possessed a bandwidth of approximately 0.4 rad/s. The design was based on the vehicle dynamics at 60 knots. Figures 4 and 5 show the resulting closed-loop transfer function for altitude rate ($\dot{h}/\dot{h}_c'$) and airspeed (u/u_c). The latter transfer function was calculated with the altitude-rate loop closed. The prime notation on h_c' serves to indicate that $h_c' \neq \mathrm{d}(h_c)\,\mathrm{d}t$. This feedback system possessed sufficient robustness to be employed for the entire flight regime studied here. Given this fact, the GPC design was also based on the 60-kt vehicle/SAS dynamics (the effective vehicle).

2-3) Figure 6 compares the actual and reduced-order h/u_{GPC} transfer functions for the vehicle plus SAS; i.e., all the feedback loops in Fig. 3 were closed in computing h/u_{GPC}. As can be seen, the reduced-order transfer function compares quite favorably with that of the actual vehicle. The reduced-order function is of order 2, while that of the actual vehicle/SAS dynamics are of order 8. The dynamics of both the actual and simplified vehicle are controllable and observable, and hence meet the conditions of the stability theorem stated previously. The reduced-order transfer function is given by

$$\frac{h}{u_{GPC}}(s) = \frac{0.8446}{s(s/4.72 + 1)} \tag{21}$$

Note that, in terms of the GPC design, $n = 3$, including the additional order arising from the inherent integral action of the GPC design. The discretization interval here was selected as $T = 0.1$ s, and was not considered a design parameter. With this interval and including the effects of a zero-order hold, the dynamics of Eq. (21) become

$$\frac{h}{u_{GPC}}(q^{-1}) = \frac{q^{-1}(0.01713 + 0.14644q^{-1})}{1 - 1.6238^{-1} + 0.62375} \tag{22}$$

4-5) The initial GPC parameters are $N_1 = n = 3$, $N_2 = 2n - 1 = 5$, $N_U = n = 3$, and $\lambda = 0$. Figure 7 shows the locus of w'-plane closed-loop characteristics roots for different λ values. Based on Fig. 7 and the corresponding step re-

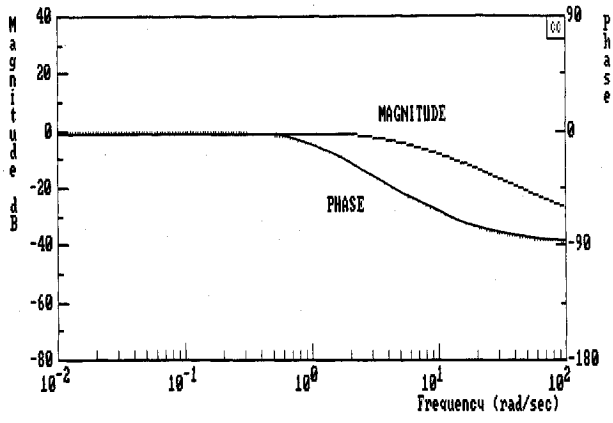

Fig. 4 The $\dot{h}/\dot{h}_c'$ transfer function for system of Fig. 3.

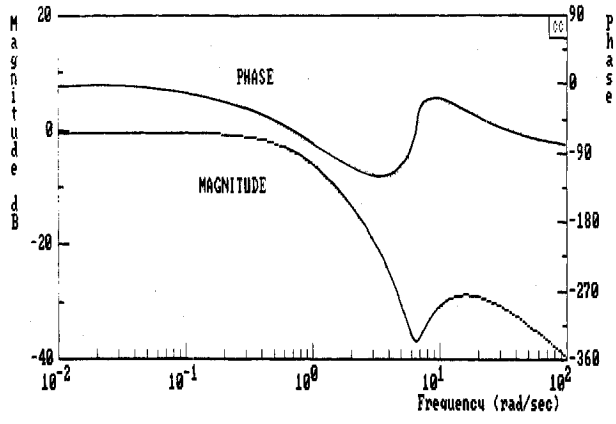

Fig. 5 The u/u_c transfer function for system of Fig. 3, altitude-rate loop closed.

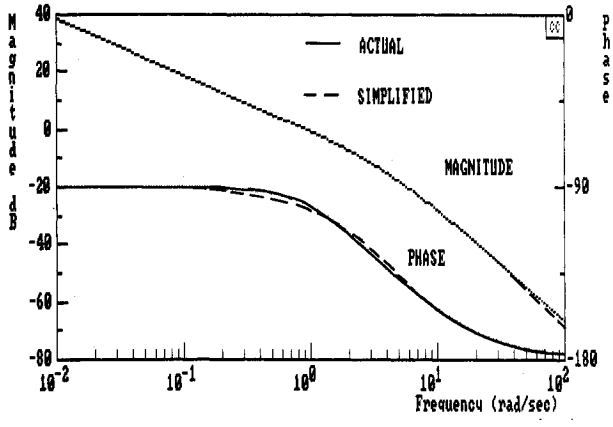

Fig. 6 Comparison of actual and reduced-order h/u_{GPC} transfer functions, calculated with all loops in Fig. 3 closed.

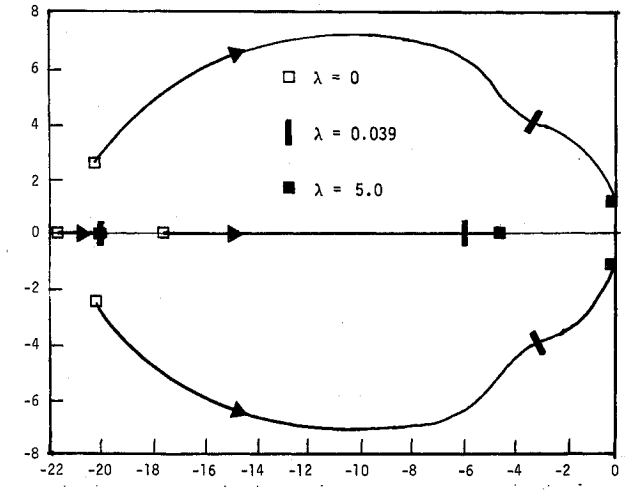

Fig. 7 The w'-plane locus of closed-loop roots of h/h_c of Fig. 3 as a function of GPC control increment weighting λ.

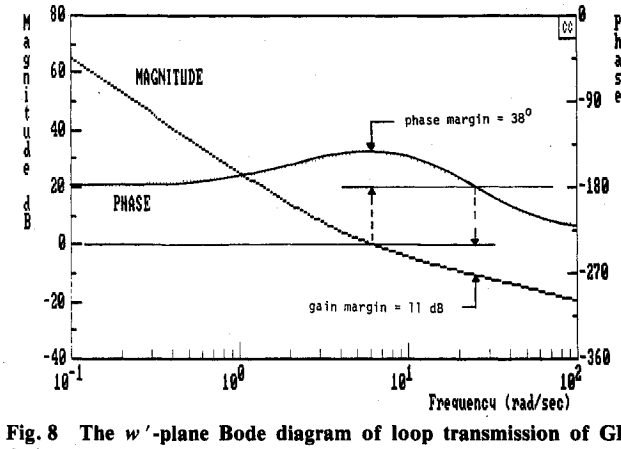

Fig. 8 The w'-plane Bode diagram of loop transmission of GPC design.

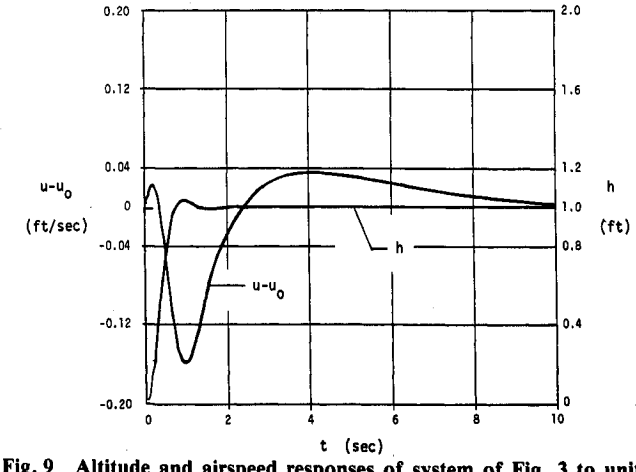

Fig. 9 Altitude and airspeed responses of system of Fig. 3 to unit step altitude command h_c.

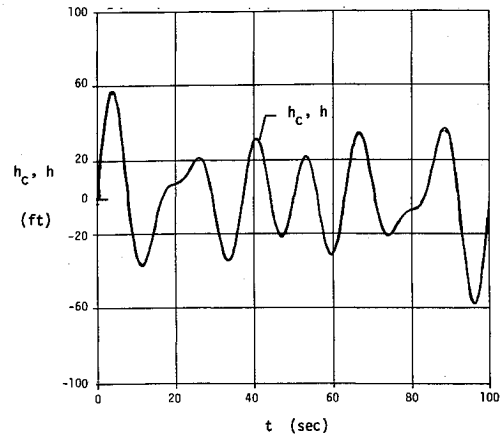

Fig. 10 Altitude tracking performance of system of Fig. 3.

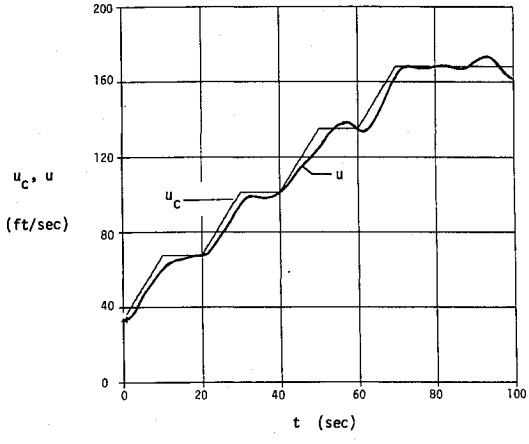

Fig. 11 Airspeed tracking performance of system of Fig. 3.

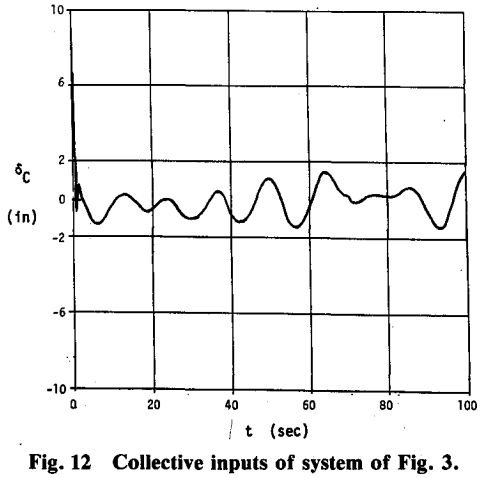

Fig. 12 Collective inputs of system of Fig. 3.

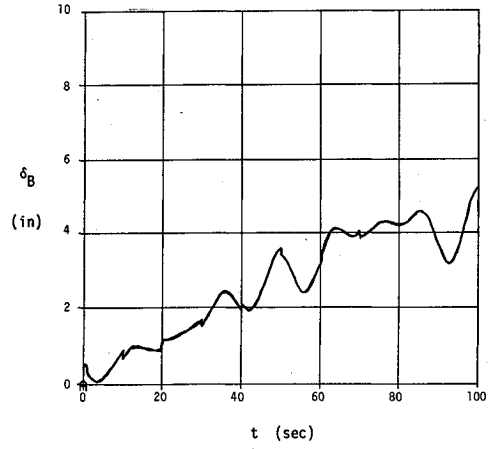

Fig. 13 Longitudinal cyclic inputs of system of Fig. 3.

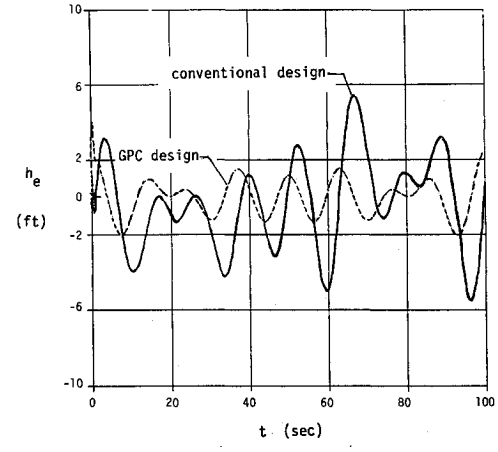

Fig. 14 Comparison of altitude tracking errors for systems of Figs. 3 and 15.

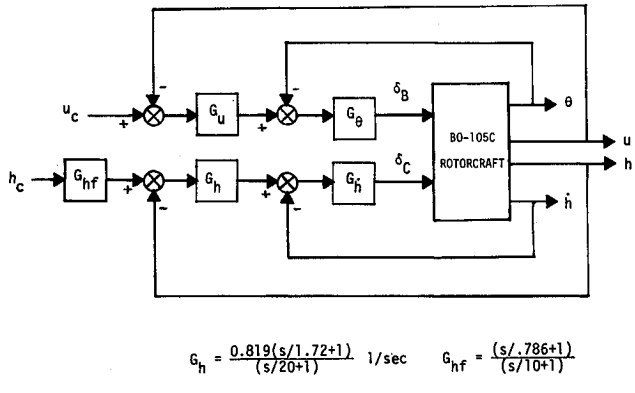

Fig. 15 Conventional control system design.

sponses, λ was selected as $\lambda = 0.039$. Figure 8 shows the w'-plane Bode plot for the loop transmission given by Eq. (19). The gain and phase margins are seen to be 38 deg and 11 dB, respectively, which were judged acceptable for this design. The maximum costing horizon of 0.5 s is quite modest. An examination of the effective vehicle dynamics for the 20- and 100-kt conditions revealed that the transfer function of Eq. (21) still provided an excellent approximation.

6) Figure 9 shows the step responses for h and u for the actual system, wherein the airspeed command has been set to 60 kts (no change). As can be seen, the transient responses are well damped.

Simulation

Figures 10–13 show the altitude, airspeed, collective, and longitudinal cyclic time histories that result when the rotorcraft is commanded to follow the altitude trajectory of Eq. (20) with the aforementioned airspeed command profile. The units on the collective and longitudinal cyclic refer to equivalent control displacement at the pilot's hand. For convenience in plotting, the control inputs were assumed to be zero when positioned at the 20-kt trim values (see the Appendix). The flight-path tracking performance is such that it is difficult to distinguish the command from the output time histories in Fig. 10; thus, the dashed curve in Fig. 14 shows the altitude errors. With the exception of the transients at the beginning and end of the run, the maximum altitude errors are seen to be less than 1.5 ft in magnitude. The increasing amplitude of the longitudinal cyclic input in Fig. 13 reflects the monotonically increasing airspeed.

It is interesting to compare the performance of the GPC system with a more conventional design. To this end, the

system of Fig. 15 was simulated. This control system is identical to the SAS design of Fig. 3, with the addition of an altitude loop, with equalization G_h and a prefilter G_{hf}. As can be seen from the figure, the prefilter essentially provides a low-frequency lead command to improve altitude tracking performance. In the absence of the prefilter, the altitude loop possessed a bandwidth of approximately 0.6 rad/s; with the prefilter, the bandwidth exceeded 10 rad/s. Of course, the tracking improvements that result from the prefilter are completely dependent on the availability of precise commanded altitude-rate information. Noise or other errors in this signal will compromise significantly the performance of this conventional design. The solid curve in Fig. 14 shows the altitude errors for this conventional design. As can be seen, the maximum altitude errors are on the order of 5 ft in magnitude, considerably larger than those for the GPC design.

Conclusions

Based on the research described herein, the following conclusions can be drawn.

1) The single-input/single-output generalized predictive control (GPC) algorithm can be applied to precise flight-path control as part of a multiloop flight control system.

2) A design procedure can be offered in which a stability augmentation system creates a simplified effective vehicle, which is then subjected to GPC control. For the purposes of design, the effective vehicle is approximated by lower order, linear, time-invariant dynamics. The lower order nature of the effective vehicle (as compared with the unaugmented vehicle) permits the implementation of a simple GPC controller.

3) Given the order of the effective vehicle dynamics, all but one of the parameters that determine the GPC controller can be selected. The final GPC parameter, the control increment weighting coefficient λ, is selected on a trial-and-error basis using the system step response with the simplified dynamics or, equivalently, via pole placement.

4) The simulation of a rotorcraft with highly coupled, time-varying, unstable, and/or nonminimum phase dynamics in a longitudinal terrain avoidance task demonstrated the potential of the GPC algorithm to provide excellent flight-path tracking performance with adequate stability margins.

Appendix: BO-105C, Longitudinal Linearized Equations of Motion (Body Axes)—Airspeeds 20–100 kt

$$\dot{u} = (X_u)u + (X_w)w + [-W_0 + X_q]q - (g\cos\theta_0)\theta + X_{\delta C}\delta_C + X_{\delta B}\delta_B$$

$$\dot{w} = (Z_u)u + (Z_w)w + [U_0 + Z_q]q - (g\sin\theta_0)\theta + Z_{\delta C}\delta_C + Z_{\delta B}\delta_B$$

$$\dot{q} = (M_u)u + (M_w)w + M_q q + M_{\delta C}\delta_C + M_{\delta B}\delta_B$$

$$\dot{\theta} = q$$

$$\dot{x} = [A]\{x\} + [B]\{u\}, \quad x = \{u,w,q,\theta\}^T, \quad u = \{\delta_C,\delta_B\}^T$$

Units

u, ft/s, w, ft/s, q, rad/s, θ, rad, δ_C, in., δ_B, in.

20 kt (U_0 = 33.73 ft/s):

$\theta_0 = 0.0361$ rad, $\delta_{C0} = 8.72$ in., $\delta_{B0} = 0.4$ in.

$$[A] = \begin{bmatrix} -0.0154 & 0.0193 & 0.6176 & -32.15 \\ -0.1978 & -0.4699 & 33.79 & -1.162 \\ 0.0204 & 0.0017 & -3.4423 & 0 \\ 0 & 0 & 1.0 & 0 \end{bmatrix}$$

$$[B] = \begin{bmatrix} 0.2412 & 0.7813 \\ -9.3763 & 0.5217 \\ 0.0823 & -0.9712 \\ 0 & 0 \end{bmatrix}$$

40 kt (U_0 = 67.49 ft/s):

$\theta_0 = 0.0284$ rad, $\delta_{C0} = 8.03$ in., $\delta_{B0} = 1.31$ in.

$$[A] = \begin{bmatrix} -0.0245 & 0.0253 & 0.1898 & -32.16 \\ -0.1277 & -0.6648 & 67.41 & -0.915 \\ 0.0223 & 0.01 & -3.4724 & 0 \\ 0 & 0 & 1.0 & 0 \end{bmatrix}$$

$$[B] = \begin{bmatrix} 0.1651 & 0.7363 \\ -10.165 & 1.111 \\ 0.2566 & -0.9717 \\ 0 & 0 \end{bmatrix}$$

60 kt (U_0 = 101.26 ft/s):

$\theta_0 = 0.0103$ rad, $\delta_{C0} = 7.89$ in., $\delta_{B0} = 2.39$ in.

$$[A] = \begin{bmatrix} -0.0338 & 0.0311 & 1.044 & -32.17 \\ -0.0564 & -0.7886 & 101.45 & -0.331 \\ 0.0179 & 0.0129 & -3.6151 & 0 \\ 0 & 0 & 1.0 & 0 \end{bmatrix}$$

$$[B] = \begin{bmatrix} 0.1583 & 0.7037 \\ -11.436 & 1.797 \\ 0.5163 & -0.9962 \\ 0 & 0 \end{bmatrix}$$

80 kt (U_0 = 135.01 ft/s):

$\theta_0 = -0.015$ rad, $\delta_{C0} = 8.13$ in., $\delta_{B0} = 3.26$ in.

$$[A] = \begin{bmatrix} -0.0423 & 0.0292 & 4.03 & -32.17 \\ -0.0158 & -0.8734 & 135.03 & 0.483 \\ 0.0153 & 0.0170 & -3.63 & 0 \\ 0 & 0 & 1.0 & 0 \end{bmatrix}$$

$$[B] = \begin{bmatrix} 0.0515 & 0.6957 \\ -12.714 & 2.563 \\ 0.7645 & -1.038 \\ 0 & 0 \end{bmatrix}$$

100 kt (U_0 = 168.58 ft/s):

$\theta_0 = -0.0489$ rad, $\delta_{C0} = 8.85$ in., $\delta_{B0} = 4.47$ in.

$$[A] = \begin{bmatrix} -0.0524 & 0.0269 & 10.12 & -32.13 \\ 0.0026 & -0.9411 & 168.43 & 1.57 \\ 0.0183 & 0.0250 & -3.60 & 0 \\ 0 & 0 & 1.0 & 0 \end{bmatrix}$$

$$[B] = \begin{bmatrix} -0.1082 & 0.7361 \\ -13.90 & 3.362 \\ 1.011 & -1.095 \\ 0 & 0 \end{bmatrix}$$

Acknowledgment

This research was supported by Grant NAG 2-221 from the Aircraft Guidance and Navigation Branch and the Flight Dynamics and Controls Branch of NASA Ames Research Center, Moffett Field, California.

References

[1]Richalet, J., Rault, A., Testud, J. L., and Papon, J., "Model Predictive Heuristic Control: Applications to Industrial Processes," *Automatica,* Vol. 14, No. 5, 1978, pp. 413–428.

[2]Rouhani, R., and Mehra, R. K., "Model Algorithmic Control (MAC): Basic Theoretical Properties," *Automatica,* Vol. 18, No. 4, 1982, pp. 401–414.

[3]Reid, J. G., Chaffin, D. E., and Silverthorn, J. T., "Output Predictive Algorithmic Control: Precision Tracking with Application to Terrain Following," *Journal of Guidance, Control, and Dynamics,* Vol. 4, No. 5, 1981, pp. 502–509.

[4]Clarke, D. W., and Zhang, L., "Long-Range Predictive Control Using Weighting Sequence Models," *IEE Proceedings,* Vol. 134, Pt. D, No. 3, 1987, pp. 187–195.

[5]Clarke, D. W., Mohtadi, C., and Tuffs, P. S., "Generalized Predictive Control, Parts I and II," *Automatica,* Vol. 23, No. 2, 1987, pp. 137–160.

[6]De Reyser, R. M. C., Van De Velde, G. A., and Dumortier, F. A. G., "A Comparative Study of Self-Adaptive Long-Range Predictive Control Methods," *Automatica,* Vol. 24, No. 2, 1988, pp. 149–163.

[7]Hess, R. A., and Jung, Y. C., "An Application of Generalized Predictive Control to Rotorcraft Terrain-Following Flight," *IEEE Transactions on Systems, Man, and Cybernetics,* Vol. 19, No. 5, 1989, pp. 955–962.

[8]Astrom, K. J., and Wittenmark, B., *Adaptive Control,* Addison-Wesley, Reading, MA, 1989, Appendix A.

[9]Clarke, D. W., and Mohtadi, C., "Properties of Generalized Predictive Control," *Automatica,* Vol. 25, No. 6, 1989, pp. 859–875.

[10]Crisalle, O. D., Seborg, D. E., and Mellichamp, D. A., "Theoretical Analysis of Long-Range Predictive Controllers," *Proceedings of the 1989 American Control Conference,* 1989, pp. 570–576.

[11]Francis, B. A., Helton, J. W., and Zames, G., "H^{∞}-Optimal Feedback Controllers for Linear Multi-Variable Systems," *IEEE Transactions on Automatic Control,* Vol. AC-29, No. 10, 1984, pp. 888–900.

[12]Horowitz, I., "Quantitative Feedback Theory (QFT)," *Proceedings of the 1988 American Control Conference,* June 1988, pp. 2032–2037.

[13]Cheng, V. H. L., and Sridhar, B., "Considerations for Automated Nap-of-the-Earth Rotorcraft Flight," *Proceedings of the 1988 American Control Conference,* June 1988, pp. 967–976.

[14]Heffley, R. K., et al., "A Compilation and Analysis of Helicopter Handling Qualities Data, Vol. 1: Data Compilation," NASA CR-3144, Aug. 1979.